A ISOPHOT Study* of the Disk of Galaxy NGC 6946: 60 μm Infrared and Radio Continuum Correlation

N. Y. Lu[1], G. Helou[1], R. Tuffs[2], C. Xu[2], S. Malhotra[1], M. W. Werner[3], and H. Thronson[4]

[1] Infrared Processing and Analysis Center, MS 10022, California Institute of Technology, Pasadena, CA 91125, U.S.A.
[2] Max-Planck Institut für Kernphysik, Saupfercheckweg 1, 1)-691 17 Heidelberg, Germany
[3] Jet propulsion Laboratory, MS 233303, California Institute of Technology, Pasadena, CA 91109, U.S.A.
[4] Wyoming Infrared Observatory, University of Wyoming, Laramie, WY 82071, and Code SR, NASA Headquarters, Washington DC 20546, U.S.A.

Received 6 August 1996; accepted

Abstract. We combine the ISOPHOT 60 μm image of Tuffs et al. (1996) and VLA radio continuum images at 6 and 20 cm from the literature to study the 60 μm light distribution and its correlation with radio continuum within the disk of nearby spiral galaxy NGC 6946, at an effective resolution of ~ 52" ($\approx$ 1.4 kpc at a distance of 5.5 Mpc). Our main results are: (1) The galaxy disk at 60 μm appears to follow an exponential form out to at least the 25th blue surface magnitude. Our best estimate of its e-folding scale length is 1'.25 $\pm$ 0'.04 which is less than that measured in radio continuum at the 3σ significance level. (2) Within the galaxy disk but outside the inner 2.4 kpc, the 60 μm-to radio continuum surface brightness ratio, Q, decreases radially outward by a factor of 1.7 on average between 1'.5 and 5'.5; the infrared and radio morphologies are quite similar; and Q is quantitatively better correlated with surface brightness than with radius. These results are consistent with previous findings based on resolution-enhanced IRAS data.

Key words: Galaxies: individual/NGC6946 - galaxies: ISM infrared: galaxies - radio continuum: galaxies

1. Introduction

IRAS has revealed a good correlation between the thermal fat-infrared (FIR) emission and the primarily non-thermal radio continuum emission for spiral galaxies (e.g., Dickey & Salpeter 1984; Helou, Soifer, & Rowan-Robinson 1985, Condon, Anderson, & Helou 1991). More detailed studies of a dozen or so nearby galaxies using IRAS HiRes images showed that the FIR-to radio surface brightness (SB) ratio, Q, generally decreases with increasing radius in these galaxies (e.g., Bicay & Helou 1990; Marsh & Helou 1993). This systematic variation of Q may play a crucial role in understanding the physics behind the global infrared - radio correlation among galaxies (Helou & Bicay 1993). Some studies however did not confirm this systematic behavior of Q (e.g., Fitt et al. 1992). This led to a question whether the observed radial drop of Q may be an artifact of the IRAS data processing. In this letter, we use new data from the Infrared Space Observatory (ISO; Kessler et al. 1996) without any resolution enhancement to show that this radial change of Q is real in NGC 6946.

Given its large angular size (D_{25} = 11'.5) and nearly face-on appearance (inclination $\approx$ 30°), the spiral galaxy NGC 6946 is among the best objects for studying the FIR light distribution (e.g., Engargiola 1991) and its correlation with radio continuum within the galaxy disk (e.g., Bicay, Helou, & Condon 1989). The high sensitivity of the ISO 1'10'1" (Lemke et al 1996) not only makes it possible to push such studies to a fainter SB and somewhat a finer angular resolution than before, but also in the case of NGC 6946, serves as an independent measurement of the shape of the radial SB profile at ~ 60 μm for which the result from the IRAS CPC observations (van Driel et al. 1995) apparently differs from that based on the co added IRAS scans (Bothun & Rogers 1992). While the SB distributions at various FIR wavelengths are discussed mainly in Tuffs et al. (1996), we limit this letter to a comparative study of the 60 μm and radio continuum emissions within the galaxy disk. We briefly describe the data in §2, discuss the infrared and radio light distributions in §3, and study the spatial variation of Q in §4, and finally give a summary in §5.

Send offprint requests to: N. Y. Lu

* Based on observations with ISO, an ESA project with instruments funded by ESA Member States (especially the PI countries: France, Germany, the Netherlands and the United Kingdom) and with the participation of ISAS and NASA.

2. Infrared and Radio Images

2.1. ISOPHOT Image at 60 μm

The 60 μm image used here was obtained by the ISOPHOT (hereafter I'1{'1') and reported in Tuffs et al. (1996), where the observational and data reduction details are also given. The overall flux calibration was done using the IRAS data. The final image has an effective angular resolution of $\sim$ 52" ($\approx$ 1.4 kpc at the distance of 5.5 Mpc of Pierce 1994) and an r.m.s. noise of about 0.7 MJy sr^{-1}.

Two potentially important systematic errors on the disk SB measurement are the stray-light contamination from the bright galaxy nucleus and the detector transient effect. The stray-light contamination at a radius of 5′ was estimated Lo be less Lhan a fcw tenths of percent of the peak response, or a level comparable to the map noise. The detector transient effect is probably significant oniy within one resolution element of the galaxy nucleus (Tuffs et al. 1996). Nevertheless, we shall roughly estimate this transient effect on the SB of the outer disk by comparing the data in the PHT in-scan direction with that in the cross-scan direction (see Tuffs et al. 1996) in §3, and derive a conservative upper limit on all possible systematic errors by a comparison with IRAS data in §2.3.

2.2. Radio Continuum Images

The radio continuum images at 6 cm and at 20 cru were taker] from Beck & Hoernes (1996) and Beck (1991), respec tively. The 6 cm radio image combined a low-resolution map from the Effelsberg telescope with a high angular resolution VI, A D-array map which has a beam size of 12 ".5 and an r.m s noise of $\sim$ 20 pJy per beam, resulting in a more accurate measurement of the total radio power. The V LA 20 cm radio image has a beam size of 42" and an r.m s. noise of $\sim 50\,\mu$Jy pcr beam. Wc have processed both radio images to be comparable to the PHT image in resolution and pixel size. The r.m.s. noises of the final radio images arc on the order of 10^{-3} MJy sr^{-1} each.

2.9. Comparison of the PHT and IRAS images

W c compared the PHT image with an IRAS image at 60 μm constructed using IPAC's HiRes software with 20 iteration steps, which should have an effective resolution of 40" to 60" and an r.m.s. noise of 0.66 MJy sr^{-1}. The result of the comparison is summarized in Table 1 which gives, for each bin in the face-on radius r_0, the number of cells (to be explained below); the mean PHT SB, $< I >$, in MJy sr^{-1}; the ratio of $< I >$ to the mean IRAS SB $<1>$; and the r.m s. of (1' -- I) in MJy sr^{-1}. In evaluating these parameters, each of the galaxy images was divided into cells of 40" x 40". The radius of each cell in the plane of the galaxy was determined using an inclination angle of 30° and a position angle of 69° (N to E). Except for $r_0 \leq$ 1′ where the PHT data are known to underestimate the true SB (Tuffs et al. 1996), the two maps agree with each other within $\sim$ 40% out to $r_0 \sim 5'$. The PHT map however is systematically brighter than the IRAS map in the outer parts of the disk. We show in §3 that this discrepancy arises mainly from the PHT data cells near the cross-scan direction In the absence of definitive evidence favoring either map, we take this discrepancy as arr upper limit Lo systematic errors affecting the PHT map and use the IRAS data for cells with $r_0 < 1.'5$ irr the remainder of this letter.

Table 1. Comparison of the ISOPHOT and IRAS images

r_0 (arcmin)	< 1	1-2	2-3	3 4	4-4.5	45-5	5-5 5
No of cells	7	18	32	42	24	30	31
$< I >$	80.0	39.5	27.2	14.9	8.9	6.7	5 0
$< I > / < I >$	0.4	0.8	1.0	0.9	1.2	1.4	2.2
r.m.s. $(I - I)$	71.9	19. s	8.3	6.3	4.2	3.1	?4

3. FI R and Radio-Continuum Light Distributions

As illustrated in Fig. 1 where the PHT image of NGC 6946 at 60 μm in grey scale is overlaid with its radio continuum image at 6 cm in contours, the overall morphological resemblance between the infrared and radio images appears to be good out to at least the last contour at r_0 - 5′.5. The isophotal shapes arc quite similar and intensity peaks outside the nucleus spatially coincide.

The radial profiles in infrared and radio continuum arc compared in Fig. 2. Each data point represents a 40" x 40" ccl] as defined above. Those filled circles arc cells whose 60 μm SB were derived from the IRAS HiRes data. open squares and crosses arc PHT data cells within 45° of the PHT in-scan and cross-scan directions (see Tuffs et al. 1996), respectively. Hereafter, wc refer to these two sampling areas simply as PHT in-scan and cross-scan directions, respectively. This allows for a check on the detector transient effect which, if present, would affect the in-scan cells much more severely than the cross scan cells. We use the radio profiles as control samples for this purpose. The mean difference between the PHT in-scan and cross-scan profiles reaches up to $\sim$ 0.21 in log scale at r $\sim$ 5' with the in-scan consistently brighter than the cross-scan at the same radius. Less than half of this difference might also be observed in the radio profiles. Thus, the memory effect could overestimate the 60 μm SB at outer radii by $\sim$ 28% in the PHT in-scan direction. In the analysis beiow, wc mainly rciy on the PHT cross-scan data Lo make our best estimates on disk properties.

Fig. 1. PHT image of NGC 6946 at 60 μm in grey scale, overlaid with contours of its radio continuum image at 6 cm. Brightnesses are displayed on a linear scale. Both images have a size of 11′ x 11′, an angular resolution of about 52", and a pixel size of 20" x 20". North is at top and East to the left.

Fig. 2. Plot of logarithmic SB as a function of the face-on radius, r_0, for the 60 μm data, and for radio continuum data at 20 cm and 6 cm. The 6 cm radio continuum data points have been shifted by −1.5 in log scale to be visually separated from the 20 cm data points. Each data point represents the mean SB within a cell of 40" x40", with open squares and crosses for cells within 45° of the 11′ in-scan and cross-scan directions (see Tuffs et al. 1996), respectively. At 60 μm, the SB in cells with a radius less than 1′.5 are derived from the IRAS data, and are plotted as filled circles. The dotted vertical line indicates $r_0 = 5'.5 (\approx D_{25}/2)$ and dashed horizontal lines schematically indicate the 3σ levels.

The galaxy disk at 60 μm appears also to follow an exponential law on average. This exponential form apparently holds even beyond the 25th Surface magnitude in blue (Tuffs et al. 1996). The e-folding scale length, from a least-squares fit to the mean radial profile over radii of $1'.5 < r_0 < 5'.5$, is $1'.65 (\pm 0'.07)$ if all the cells are used, or $1'.25 (\pm 0'.04)$ if only the cross scan rolls are used. The former value can be safely taken as an upper limit on the true scale length. A similar fit to the 6 cm and 20 cm radio profiles in the 11′ cross-stall direction yielded a scale length of $1'.50 (\pm 0'.07)$ each. Thus, the disk e-folding scale length at 60 μm is significantly less than that measured in optical (> 1′.7; Ables 1971; Engargiola 1991), and is also less than that in radio continuum at a significance level of 3σ. Variations of scale length with wavelength similar to that in NGC 6946 were also found in other nearby galaxies using IRAS data (e.g., Rice et al. 1990).

4. Spatial Variation of the FIR-to-Radio Ratio

We define Q_{20cm} (Q_{6cm}) to be a dimensionless ratio of the SB at 60um to that at 20 cm (6 cm). The spatial variation of Q is illustrated in Fig. 3 as a function of the face-on radius, and in Fig. 4 by plotting Q_{20cm} as a function of the SB at 6 cm. The symbols of the data points in these figures are coded in the same way as in Fig. 2, but points are plotted here only for $r_0 < 5'.5$, where all the data points are still well above the 3σ levels (see Fig. 2) and the systematic errors are likely to be less than 50% (see §2.3).

Fig. 3. Plots of the far-infrared to radio continuum ratio, Q, as a function of the logarithmic face-on radius r_0. The upper panel shows 60 μm to 20 cm, while the lower panel shows 60 μm to 6 cm. The symbols are the same as in Fig. 2, but only data cells with $r_0 < 5'.5$ are plotted here. The solid line in each panel indicates the mean radial profile of Q based on all the data points in a given radial bin. Also shown are 1σ error bars for the means, estimated from the scatter of the data points in the figure.

Fig. 4. Plot of Q_{20cm} as a function of the SB at 6 cm. Only IRAS data and 1'11'1' cross-scan data points are shown here. The symbols are the same as in Fig. 2. The solid line indicates how the mean of Q_{20cm} varies as the 6 cm SB changes. Also shown are 1σ error bars for the means as defined in Fig. 3.

Some numerical results and implications can be drawn from Figs 3 and 4: (1) For $1'.5 \lesssim r_0 \lesssim 5.'5$, the 1'1['1' data show that Q decreases radially out by a factor of $\sim 1.3(\pm 0.08)$ on average, as indicated by the solid line in Fig. 3. However, a better estimate using the PHT cross-scan data points shows Q dropping by a factor of $\sim 1.7(\pm 0.05)$ over the same radii. Since this radial gradient of Q is likely to continue in the inner disk of $r_0 < 1.'5$, we conclude that within the disk of the galaxy, Q decreases radially out by at least a factor of 1.7 on average. (2) The radial profile of Q in the outer part of the galaxy disk ($r_0 \gtrsim 4'$) suggests a "flattening out." However, this comes mostly from the 1'11'1' in-scan data points. The cross-scan data show mainly a larger dispersion in Q. (3) Fig. 4 shows that Q is also correlated with SB on average. As the 6 cm SB decreases, the same 1'11'1' cross-scan data as used in Fig 3 shows an average drop by a factor of $3.6^{+1.7}_{-1.1}$ in Fig. 4. This steeper dependence of Q on SB suggests that the correlation of Q with SB is probably more physically significant than with the radius.

These results are in agreement with the description of the radio disk as a "smeared" version of the infrared disk of a galaxy (Bicay & Helou 1990). Each local maximum in disk brightness adds dispersion to the plot of Q *vs.* radius, but is a local center of star formation from which Q decreases radially. The radio disk arises primarily from synchrotron emission by cosmic ray electrons in the galaxy's magnetic field, whereas dust heated by stars defines the infrared disk. Cosmic ray electrons can diffuse away from their sources as much as a kpc before decaying radiatively; heating photons on the other hand will typically get absorbed and re-emitted in the infrared within a hundred pc of their source. Assuming that both radiating electrons and heating photons originate in the same sites of star formation, this difference in radiating scale length explains the "smearing" relation between infrared and radio disks (Helou & Bicay 1993).

5. Summary

We have used a new 1'1['1' image at 60 μm of the galaxy NGC 6946 to show: (1) The galaxy disk at 60 μm follows an exponential fall-off out to at least the 25th blue surface magnitude. Our best estimate of its e-folding scale length is $1'.25 \pm 0'.04$ which is less than that measured in radio continuum at the 3σ significance level. (2) Within the 25th blue surface magnitude of the galaxy disk, but outside the inner 2.4 kpc (assuming a distance of 5.5 Mpc), the 60 μm-to radio continuum surface brightness ratio, Q, decreases radially out by a factor of 1.7 on average; the infrared and radio morphologies appear quite similar; and Q is quantitatively better correlated with surface brightness than with radius. These 1S01'110"1' results are consistent with previous findings based on resolution-enhanced IRAS data (e.g., Marsh & Helou 1995).

Acknowledgements. We wish to thank R. Beck for providing us with the radio images and C. Gabriel for helpful conversations on the 1S01'110'1' data reduction. This work was supported in part by ISO data analysis funding from the US National Aeronautics and Space Administration, and carried out at the Infrared Processing and Analysis Center and the Jet Propulsion Laboratory of the California Institute of Technology.

References

Ables, H. 1). 1971, Pub US Naval Obs., Ser. 2, Vol. 20, Pt 4.
Aumann, H. H., Fowler, J. W., & Melnyk, M. 1990, AJ, 99, 1674
Beck, R. 1991, A&A, 251, 15.
Beck, R., & Hoernes, P. 1996, Nat, 379, 47.
Bicay, M. 1)., & Helou, G. 1990, ApJ, 362, 59.
Bicay, M. D., Helou, G., & Condon, J. J. 1989, Ap J, 338, L53
Bothun, G. D., & Rogers, C. 1992, AJ, 103, 1484.
Condon, J. J., Anderson, M. L., & Helou, G. 1991, ApJ, 376, 95.
Dickey, J. M., & Salpeter, E. E. 1984, AJ, 284, 461.
Engargiola, G. 1991, ApJS, 76, 875.
Fitt, A. J., Howarth, N. A., Alexander, 1'., & Lasenby, A. N. 1992, MNRAS, 255, 146.
Helou, G., & Bicay, M. 1993, AI, J, 415, 93.
Helou, G., & Soifer, B. T., & Rowan-Robinson, M. 1985, ApJ, 298. L7.
Kessler, M., et al. 1996, A&A (this volume).
Lemke, D., et al. 1996, A&A (this volume).
Marsh, K. A., & Helou, G. 1995, ApJ, 445, 599.
Pierce, M. 1994, Ap J, 430, 53.
Rice, W. et al. 1988, ApJS, 68, 91.
Rice, W., Boulanger, F., Viallefond, F., Soifer, B. T., & Freedman, W. L. 1990, ApJ, 358, 418.
Tuffs, R. et al. 1996, A&A (this volume).
van Driel, W., Valentijn, E. A., Wesselius, P. R., & Kussendrager, D. 1995, A&A, 298, L41.

This article was processed by the author using Springer-Verlag LaTeX A&A style file *L-AA* version 3.

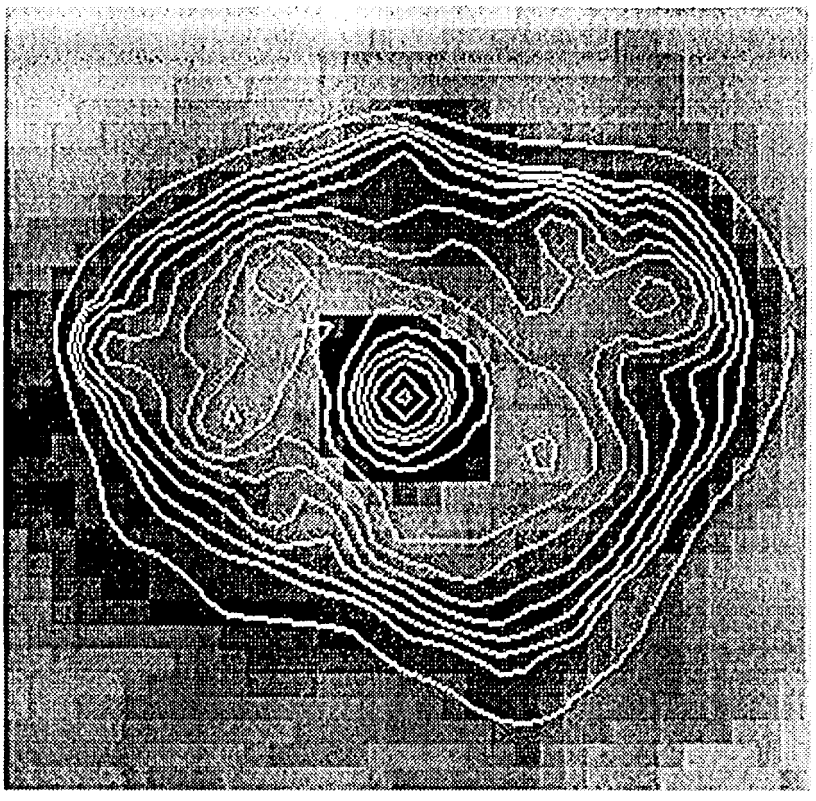

Figure 1

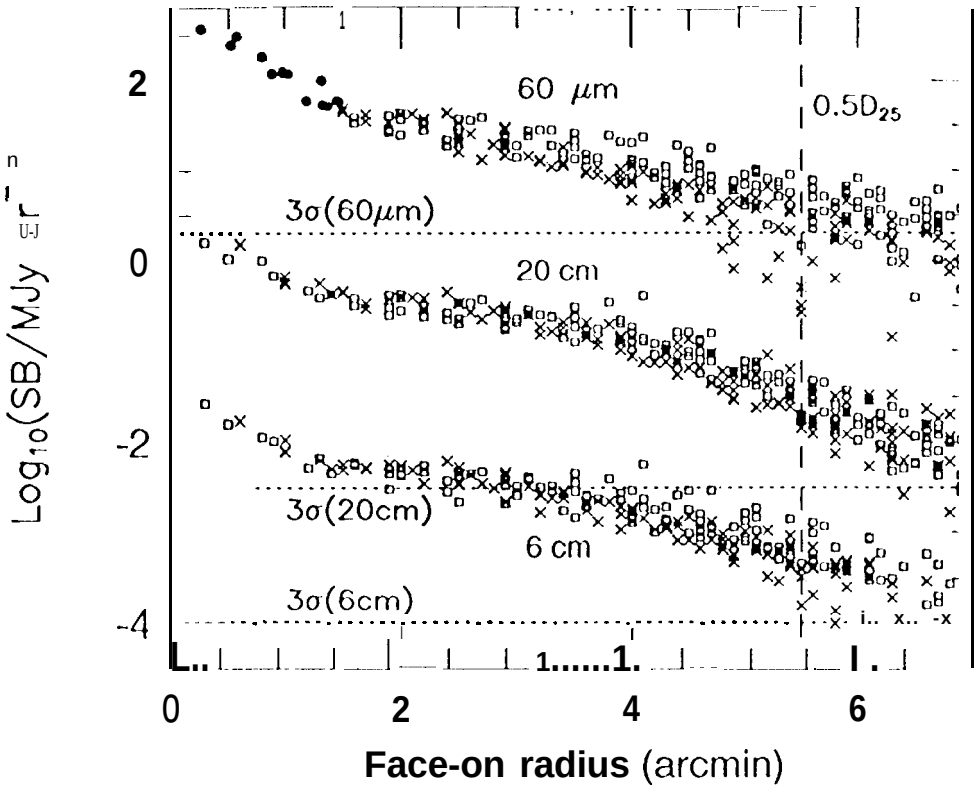
60 μm
0.5D25
3σ(60μm)
20 cm
3σ(20cm)
6 cm
3σ(6cm)
2
0
-2
-4
0
2
4
6
Log10(SB/MJy sr-1)
Face-on radius (arcmin)

Figure 2

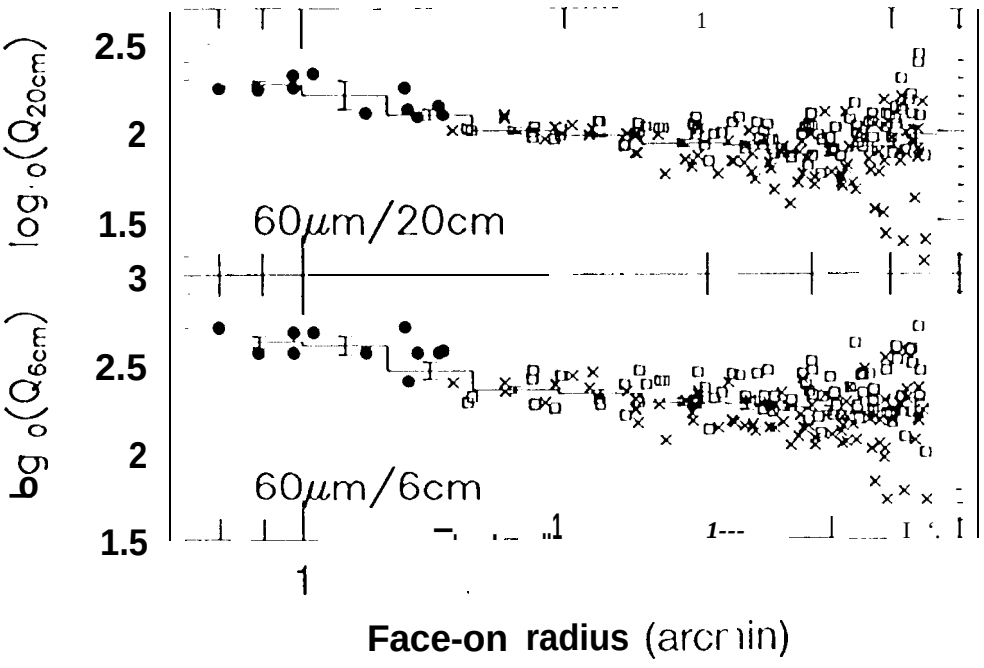
2.5
2
1.5
3
2.5
2
1.5
60μm/20cm
60μm/6cm
log10(Q20cm)
log10(Q6cm)
Face-on radius (arcmin)

Figure 3

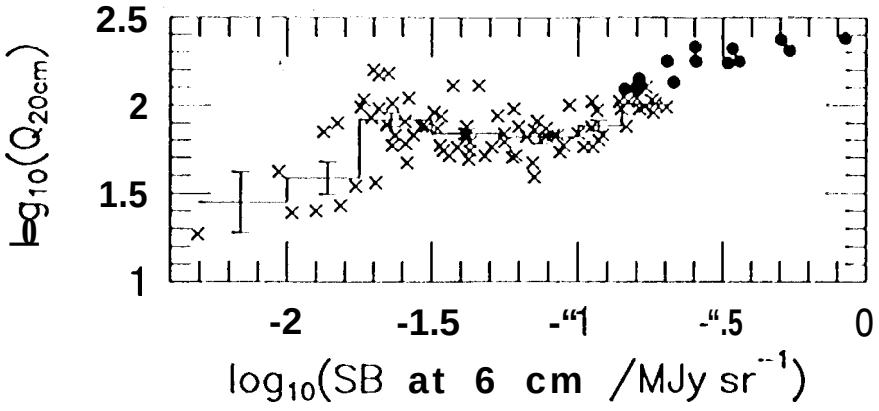

Figure 4